J. Fluid Mech. (2016), *vol.* 796, *pp.* 712–731.

doi:10.1017/jfm.2016.272

Merging of two or more plumes arranged around a circle

G. G. Rooney†

Met Office, FitzRoy Road, Exeter EX1 3PB, UK

(Received 2 July 2015; revised 8 February 2016; accepted 12 April 2016;
first published online 11 May 2016)

A model is presented of merging turbulent plumes from sources evenly spaced around a horizontal circle in a quiescent, unstratified background. This follows the previously developed method of (i) identifying the boundaries of interacting plumes with velocity-potential contours of line sinks and (ii) closing the generalised plume equations with an entrainment assumption based on the integrated flux across the plume boundaries. It includes the simplest case of two merging plumes, as well as being applicable to plume flows in restricted corner configurations. The model is shown to display the expected limiting behaviour for the source plumes and the merged plume. Consideration of the plume fluxes in the merging region leads to a revision of the entrainment assumption. The resulting revised model compares satisfactorily with previous estimates of volume flux in two merging plumes.

Key words: convection, plumes/thermals

1. Introduction

Many studies of naturally ventilated spaces have followed upon the important work of Linden, Lane-Serff & Smeed (1990). These have often dealt with turbulent plume flow in a man-made enclosure. However the interactions of plumes with other plumes and with boundaries, which often occur in such spaces, are still not fully understood. In this context, Rooney (2015) proposed that symmetric plume interactions may emulate plume–boundary interactions, in the sense of the method of images. This idea allows both types of flow to be modelled in a single framework. The method was applied by Rooney (2015) to plume flow in a restricting channel.

Here, the model is extended to look at plume sources evenly spaced around a circle, with flow in the direction normal to the plane of the circle. This includes the simplest case of two interacting plumes. Under the method of images, this model also represents plume interaction with a wall and, if the symmetry is not broken, the case of a plume in a corner of angle $2\pi/n$ where n is the number of plumes. The study of these flows is highly relevant to the building ventilation problem as well as to numerous other applications, for example fire safety (Babrauskas 1980) and the melting of ice shelves (Kimura *et al.* 2014).

Several previous studies have examined the problem of merging plumes. Davidson, Papps & Wood (1994) modelled buoyant jet merging in a long row of sources by simply superimposing the velocity distributions of each jet without considering

† Email address for correspondence: gabriel.rooney@metoffice.gov.uk

interaction effects. Kaye & Linden (2004) subsequently proposed a model for the case of two plumes from point sources, in which the plumes retained circular cross-sections up to the point of merging, and plume interaction was modelled through deflection of the plume axes by mutual entrainment. This model obtained a prediction for the merging height, defined as the height at which the buoyancy distribution no longer has two separate maxima. Beyond the merging point, the flow was then modelled as a single axisymmetric plume. The predicted merging height was somewhat greater than that observed in accompanying experiments, a result attributed in part to sensitivity of the model to the plume entrainment constant. Cenedese & Linden (2014) extended this model with the introduction of an intermediate region where the plumes overlap but are not yet fully merged. The model predictions compared favourably with measurements of the volume flux (inferred from interface movement) in two merging plumes obtained from 'filling-box' experiments, although these results are also sensitive to the entrainment constant, as will be discussed later.

Other integral models have been developed on similar principles to the works already discussed. For example, Yannopoulos (2010) modelled groups of buoyant jets with an integral approach which included the superposition of concentration profiles, and closed the model with the assumption of linear plume growth. This predicted a merging height for two plumes approximately twice the distance observed by Kaye & Linden (2004). Circular arrays of multiple buoyant jets were also modelled by Lai & Lee (2012) using a semi-analytical approach. Like the other models described, this did not allow for the distortion of individual plume cross-sections, but did represent the field external to the jets as an irrotational flow based on a distribution of point sinks.

A Lagrangian model of plume rise was used by Alessandrini, Ferrero & Anfossi (2013) to simulate the flow from two plume sources aligned along a constant horizontal wind. In this approach, an unknown drag coefficient is the equivalent of the entrainment constant of Eulerian modelling. This method was used to predict concentration fields in plume dispersion, and in this case produced a smoothly evolving prediction of rise height in the merging plume. However, it is unclear whether implementation of a virtual plume origin was also required. Such flows have also been simulated using finite element methods (e.g. Mokhtarzadeh-Dehghan, König & Robins 2006). Compared to either of these methods, the integral approach taken here is potentially less computationally expensive.

Following Rooney (2015), the present model is constructed by first considering the velocity potential and entrainment of a circular group of line sinks (§ 2). The contours of velocity potential are the template for the growth of the plume–ambient boundary as the plume area increases with height. In § 3 an interacting-plume model is developed based on this. The integration of this model is discussed in §§ 4 and 5 then proposes a refinement of the model based on the balance of plume fluxes in the merging region. In § 6 the two-plume case is compared with the measurements of Cenedese & Linden (2014) in the merging region, and finally § 7 gives a concluding summary and discussion.

2. Sinks in a circle

2.1. *Complex potential*

The complex potential of a line sink of strength $-m(z)$ at the origin is

$$\Omega = -\frac{m}{2\pi}\ln Z, \tag{2.1}$$

where $Z = x + \mathrm{i}y = r\mathrm{e}^{\mathrm{i}\theta}$.

Kaye & Linden (2004) used line sinks to represent the entrainment/attraction field of two interacting plumes (see also Taylor (1958) and Turner (1973, § 6.1.1)). Extending this, the potential due to n equal line sinks, equally spaced around a circle of radius R, can be represented as

$$\Omega = -\frac{m}{2\pi}\ln(Z'^n - 1) - \frac{m}{2\pi}\ln R^n + \Pi, \tag{2.2}$$

where $Z' = x/R + \mathrm{i}y/R$ and Π is an arbitrary constant. The positions of the line sinks in Z'-space are those of the nth roots of unity. An diagram of the system is given in figure 1.

It is convenient to work with (2.2) in polar coordinates (ρ, θ), in which $Z' = \rho \mathrm{e}^{\mathrm{i}\theta}$ and $\rho = r/R$. It is also sufficient to consider only the sector containing unity, $-\pi/n \leqslant \theta \leqslant \pi/n$.

The velocity components u and v may be obtained from the complex derivative, $\mathrm{d}\Omega/\mathrm{d}Z = u - \mathrm{i}v$. In this case,

$$\begin{aligned}\frac{\mathrm{d}\Omega}{\mathrm{d}Z} &= \frac{1}{R}\frac{\mathrm{d}\Omega}{\mathrm{d}Z'} \\ &= -\frac{m}{2\pi R}\left(\frac{nZ'^{n-1}}{Z'^n - 1}\right) \\ &= -\frac{m}{2\pi R}\frac{n\rho^{n-1}[(\rho^n\cos\theta - \cos(n-1)\theta) - \mathrm{i}(\rho^n\sin\theta + \sin(n-1)\theta)]}{\rho^{2n} - 2\rho^n\cos n\theta + 1}.\end{aligned} \tag{2.3}$$

The flow speed is given by $q = |\mathrm{d}\Omega/\mathrm{d}Z|$, hence

$$q^2 = \frac{m^2}{4\pi^2R^2}\frac{n^2\rho^{2n-2}}{\rho^{2n} - 2\rho^n\cos n\theta + 1}. \tag{2.4}$$

Contours of equal velocity potential are given by $|Z'^n - 1| = k$, where k is constant. This simplifies to

$$\rho^{2n} - 2\rho^n\cos n\theta + 1 = k^2. \tag{2.5}$$

Hence

$$\rho = (\cos n\theta \pm (k^2 - \sin^2 n\theta)^{1/2})^{1/n}, \tag{2.6}$$

the negative square root being applicable for $k < 1$, or alternatively

$$\theta = \pm\frac{1}{n}\cos^{-1}\left(\frac{\rho^{2n} + 1 - k^2}{2\rho^n}\right). \tag{2.7}$$

A set of contours for the example of $n = 4$ is plotted in figure 2.

Differentiating (2.5) gives

$$\frac{\mathrm{d}\rho}{\mathrm{d}\theta} = \frac{\rho\sin n\theta}{\cos n\theta - \rho^n}. \tag{2.8}$$

Thus the maximum radial extent of each contour is at $\theta = 0$,

$$\rho_{max} = (k+1)^{1/n}. \tag{2.9}$$

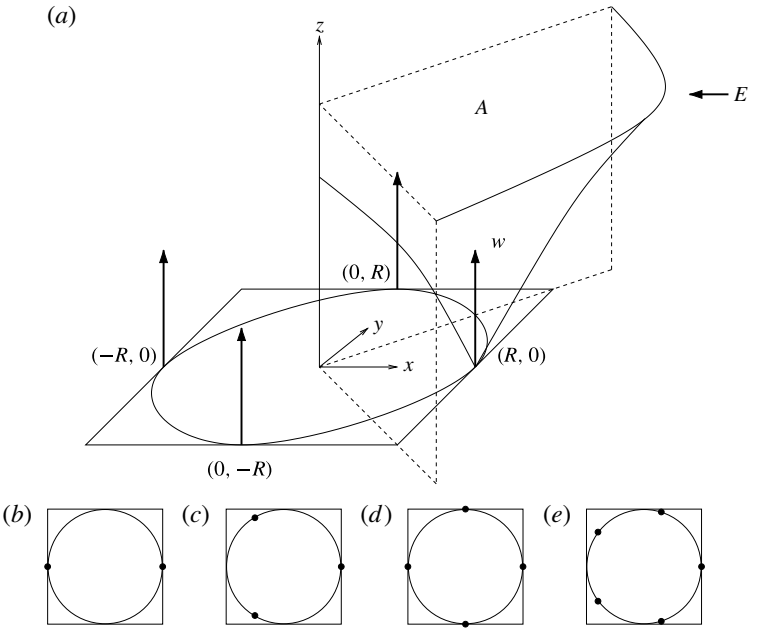

FIGURE 1. (*a*) A diagram of the situation considered, in the case $n = 4$. Cartesian (x, y) coordinates of the plume sources are marked around the notional circle of radius R. The analysis describes the flow from the source at $(R, 0)$, within the sector bounded by vertical planes of symmetry (indicated in outline by dashed lines). A is the horizontal plume area in this sector, w is the vertical plume velocity and E is the sector flux of entrained fluid across the plume–ambient boundary. All these are height dependent. A further illustration of the system, based on the results of the model presented herein, is given in figure 7. (*b–e*) Positions of plume sources around the circle in the cases $2 \leqslant n \leqslant 5$.

The angular position of the minimum contour radius depends on the value of k, being at $\theta = 0$ for $k < 1$, at $\theta = \pm\pi/n$ for $k > 1$ and undefined (at the origin) for $k = 1$. Its value is

$$\rho_{min} = \begin{cases} (1-k)^{1/n}, & k \leqslant 1 \\ (k-1)^{1/n}, & k > 1. \end{cases} \tag{2.10}$$

Thus in Z'-space, for small values of k the contours approach circles centred at $(1, 0)$ with radius k/n, and for large values of k they approach circles centred at $(0, 0)$ with radius $k^{1/n}$. In Z-space these radii will then be Rk/n and $Rk^{1/n}$, respectively.

For $k \leqslant 1$, the contours do not span the full angular range of the sector. The positions of the limits $(\rho_{lim}, \theta_{lim})$ will be given by $\mathrm{d}\theta/\mathrm{d}\rho = 0$, hence (2.8) gives ${\rho_{lim}}^n = \cos n\theta_{lim}$. Substituting into (2.5) gives the position of the angular limits to be

$$\rho_{lim} = (1-k^2)^{1/2n}, \tag{2.11}$$

$$\pm\theta_{lim} = \pm\frac{1}{n}\sin^{-1} k, \tag{2.12}$$

and hence the maximum closed-contour extent is $-\pi/2n \leqslant \theta \leqslant \pi/2n$ for $k = 1$.

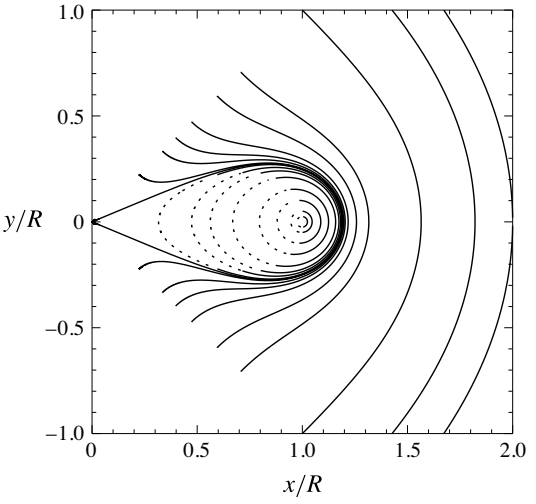

FIGURE 2. Contours of velocity potential in the sector of Z'-space containing unity, for $n=4$. The contours 'expand' from the point (1, 0) to correspond with values of k from the set {0.1, 0.2, 0.4, 0.6, 0.8, 0.9, 0.95, 0.99, 1.0, 1.01, 1.05, 1.1, 1.2, 1.5, 2.0, 5.0, 10.0, 15.0}, see (2.6). The solid and dotted parts of the closed contours ($k \leqslant 1$) indicate the positive and negative square roots in (2.6) respectively. The $k=1$ contour extends to the origin.

2.2. *Flow speed on contours*

From (2.4) and (2.5) the flow speed on (and orthogonal to) contours is

$$q = \frac{m}{2\pi R}\frac{n\rho^{n-1}}{k}. \tag{2.13}$$

The flow speed q_e at the maximum radial extent (on the line of symmetry $\theta=0$) may be obtained from (2.9) and (2.13),

$$\frac{2\pi R q_e}{m} = \frac{n(k+1)^{(n-1)/n}}{k}, \tag{2.14}$$

so that the flow speed at any point on the plume boundary may be given relative to the speed at the point $(\rho_{max}, 0)$ by

$$\frac{q}{q_e} = \frac{\rho^{n-1}}{(k+1)^{(n-1)/n}}. \tag{2.15}$$

Hence $q \leqslant q_e$ at all points on a contour.

2.3. *Flux and area integrals*

The line element $\mathrm{d}\ell$ is defined by $\mathrm{d}\ell^2 = \mathrm{d}r^2 + r^2\,\mathrm{d}\theta^2$, or in dimensionless form

$$\mathrm{d}\ell'^2 = \mathrm{d}\rho^2 + \rho^2\mathrm{d}\theta^2. \tag{2.16}$$

Given the orthogonality of streamlines and velocity-potential contours, the volume flux per unit height E across any velocity-potential contour C is then

$$E = \int_C q\,\mathrm{d}\ell = \frac{m}{2\pi}\frac{n}{k}\int_C \rho^{n-1}\,\mathrm{d}\ell'. \tag{2.17}$$

For this configuration of a finite number of line sinks, it can be shown (see appendix A) that $E = m$, independent of n or k. Thus the entrainment flux for one sector is simply m.

The area element is $\mathrm{d}A = r\,\mathrm{d}r\,\mathrm{d}\theta$. For $k > 1$ the sector area A enclosed by a contour can be obtained as

$$\frac{A}{R^2} = A' = \frac{1}{2}\int_{-\pi/n}^{\pi/n} {\rho_+}^2\,\mathrm{d}\theta, \tag{2.18}$$

where $\rho_\pm$ refer to the different solutions of (2.6). For $k \leqslant 1$ it is simpler to calculate the area within a closed contour as

$$A' = 2\int_{\rho_{min}}^{\rho_{max}} \theta_+\rho\,\mathrm{d}\rho, \tag{2.19}$$

where $\theta_\pm$ refer to the different solutions of (2.7), and $2\theta_+ = \theta_+ - \theta_-$.

3. Plumes in a circle

3.1. *Merging-plume model*

The generalised plume equations in an unstratified environment are (Rooney 2015)

$$A\frac{\mathrm{d}}{\mathrm{d}z}\left(\frac{1}{2}w^2\right) = Ag' - wE, \tag{3.1a}$$

$$\frac{\mathrm{d}}{\mathrm{d}z}(Aw) = E, \tag{3.1b}$$

where w is the top-hat vertical velocity, g' is the reduced gravity and the conserved buoyancy flux in one sector is $B = Awg'$. The properties of velocity-potential contours, which are flow orthogonal and connect points at which equal pressure impulse is required to bring about the external irrotational flow field (Batchelor 1967, § 6.10), make them good candidates for defining the time-mean outline of interacting plumes at various stages of development (Rooney 2015). In addition, a closing entrainment assumption is required. The simplest assumption is

$$q_e = \alpha w. \tag{3.2}$$

This matches the single-plume equivalents for small and large k, when the entrainment velocity is uniform on the plume boundary at any given height (and will be assessed further in § 5). From (2.14), (3.2) implies

$$(E =)m = \alpha w R f_e, \tag{3.3}$$

where $\alpha \approx 0.1$ is the entrainment constant, and

$$f_e = \frac{2\pi k}{n(k+1)^{(n-1)/n}} \longrightarrow \begin{cases} \dfrac{2\pi k^{1/n}}{n}, & k \gg 1 \\ \dfrac{2\pi k}{n}, & k \ll 1. \end{cases} \tag{3.4}$$

As expected, Rf_e tends to 2π times the plume radius in the limit of small k and tends to $2\pi/n$ times the plume radius in the limit of large k.

Equations (3.1) may be recast in terms of w and the volume flux $V = Aw$, instead of w and A. Combining this with non-dimensionalisation using the buoyancy flux B and a source length scale x_0 (to be specified further in § 4),

$$w = \alpha^{-1/3} B^{1/3} x_0^{-1/3} \bar{w}, \quad V = \alpha^{-1/3} B^{1/3} x_0^{5/3} \bar{V}, \quad z = \alpha^{-1} x_0 \, \bar{z}, \tag{3.5a–c}$$

yields the dimensionless plume equations

$$\frac{\mathrm{d}\bar{w}}{\mathrm{d}\bar{z}} = \frac{1}{\bar{w}\bar{V}} - \frac{\bar{R}\bar{w}^2}{\bar{V}} f_e, \quad \frac{\mathrm{d}\bar{V}}{\mathrm{d}\bar{z}} = \bar{R}\bar{w} f_e, \tag{3.6a,b}$$

where $\bar{R} = R/x_0$. The non-dimensionalisation (3.5) then also implies that $\bar{V}/\bar{w} = x_0^{-2} A = \bar{A}$.

The model of two merging plumes developed by Kaye & Linden (2004) assumed that each plume maintained a circular cross-section without distortion. Mutual plume attraction was included in that model, which had the effect of approximately accounting for plume distortion. This feature reduced the predicted merging distance to a value more in accord with observations. The observations and model simulations of merging-plume concentrations presented by Kaye & Linden (2004, figure 13) and Lai & Lee (2012, figure 9*a*) indicate, however, that the actual deflection of the plume centres may be quite small. In addition, it should be noted that the present model, like that of Kaye & Linden (2004), has a stagnation point between the plumes, so that distortion effects are mainly caused by restricted entrainment rather than the entrainment of one plume by another. For these reasons, plume distortion is taken to be the main mechanism of plume interaction, and it will be assumed that $\mathrm{d}R/\mathrm{d}z = 0$. It may also be noted that with this model, to take the case of two plumes as an example, each plume originates at $\rho = 1$, but at the point of merging ($k = 1$) it occupies the interval $0 \leqslant \rho \leqslant \sqrt{2}$. Thus to an observer, the plume centre may appear to have been deflected 'inward' to approximately $\rho = 0.7$ by this point.

Equations (3.6) can then be solved numerically to model plume merging in this configuration. The solution requires the use of an inverting technique to recover k from the value of A' ($= \bar{A}/\bar{R}^2$).

3.2. *Near- and far-field limits*

In the far-field limit ($k \gg 1$),

$$\alpha w R f_e \to \frac{2\pi\alpha w R k^{1/n}}{n}, \tag{3.7a}$$

$$\frac{V}{w} = A \to \frac{\pi R^2 k^{2/n}}{n}, \tag{3.7b}$$

since, as indicated above, the area tends to that of a sector of a circle with radius $Rk^{1/n}$. Hence the plume equations (3.1) tend to

$$\frac{\mathrm{d}}{\mathrm{d}z}(Vw) = \frac{B}{w}, \quad \frac{\mathrm{d}V}{\mathrm{d}z} = 2\alpha \left(\frac{\pi}{n}\right)^{1/2} V^{1/2} w^{1/2}. \tag{3.8a,b}$$

From these, the far-field similarity solution is therefore

$$w = \frac{5}{6}\left(\frac{9}{10}\right)^{1/3} \pi^{-1/3} \alpha^{-2/3} (nB)^{1/3} z^{-1/3}, \tag{3.9a}$$

$$V = \frac{1}{n}\frac{6}{5}\left(\frac{9}{10}\right)^{1/3} \pi^{2/3} \alpha^{4/3} (nB)^{1/3} z^{5/3}. \tag{3.9b}$$

Equation (3.9*b*) shows that the sum of the sector volume fluxes equals the volume flux from a single source of strength nB in this limit. Cenedese & Linden (2014) have introduced the concept of 'effective entrainment' with a parameter α_{eff} which depends on height, to relate the volume flux in merged plumes to that from the same number of isolated plumes. In the present framework, this is the same as comparing the volume flux in one sector with that for a single-plume system, $n=1$. From (3.9*b*) and following Cenedese & Linden (2014),

$$\begin{aligned}\alpha_{eff}/\alpha &= (V/V_{(n=1)})^{3/4} \\ &\to n^{-1/2}, \quad k \gg 1.\end{aligned} \tag{3.10}$$

Plume merging thus has a large effect on the eventual volume flux in the far field.

Using the non-dimensionalisation (3.5), the similarity solution (3.9) becomes

$$\bar{w} = \frac{5}{6}\left(\frac{9}{10}\right)^{1/3}\left(\frac{n}{\pi}\right)^{1/3}\bar{z}^{-1/3}, \quad \bar{V} = \frac{6}{5}\left(\frac{9}{10}\right)^{1/3}\left(\frac{n}{\pi}\right)^{-2/3}\bar{z}^{5/3}. \tag{3.11a,b}$$

Similarly, in the near-field limit ($k \ll 1$) recall that the area approaches that of a circle of radius Rk/n, and so

$$\alpha w R f_e \to \frac{2\pi\alpha w R k}{n}, \tag{3.12a}$$

$$\frac{V}{w} = A \to \pi\left(\frac{Rk}{n}\right)^2. \tag{3.12b}$$

Thus the plume equations (3.1) tend to

$$\frac{\mathrm{d}}{\mathrm{d}z}(Vw) = \frac{B}{w}, \quad \frac{\mathrm{d}V}{\mathrm{d}z} = 2\alpha\pi^{1/2}V^{1/2}w^{1/2}. \tag{3.13a,b}$$

The near-field similarity solution is thus the same as that for the far field, but with $n=1$ substituted.

3.3. *Flux-balance parameters*

For small values of k, each plume is expected to be approximately axisymmetric. In this case, the flux-balance parameter describing the departure from the plume similarity solution in the near-source region is

$$\Gamma(z) = \frac{5}{8\pi^{1/2}\alpha}\frac{BV^2}{M^{5/2}} = \frac{5}{8\pi^{1/2}}\bar{A}^{-1/2}\bar{w}^{-3}, \tag{3.14}$$

(Hunt & Kaye 2005) where $M = Vw$ is the plume momentum flux. The plume source condition is denoted $\Gamma_0 = \Gamma(0)$. $\Gamma = 1$ for a single plume in which the fluxes are in balance with the similarity solution (a so-called pure plume), while $\Gamma \to 1$ as $z \to \infty$ for a single plume with non-pure source conditions i.e. $\Gamma(0) \neq 1$.

When the plumes merge, then the sector fluxes B, V and M represent only a fraction $1/n$ of the total plume fluxes, and so the flux-balance parameter for the merged-plume system is given by

$$\Gamma_m(z) = n^{1/2}\Gamma(z). \tag{3.15}$$

It is thus expected that $\Gamma_m \to 1$ as $z \to \infty$. Since Γ_m is simply a multiple of Γ, its value can be evaluated even before the merging point. In the near field it may be interpreted as a property of the system of n plumes rather than of the merged plume.

As indicated above, a single plume from a pure source should remain pure throughout its trajectory, since it will continue to satisfy the plume similarity solution at all points. For one plume in the merging system however, even if it has a source condition of $\Gamma_0 = 1$ it has been shown above that it will eventually depart from the single-plume similarity solution. Nonetheless, if the plumes which merge are pure at the source ($\Gamma_0 = 1$), then the function

$$f_m = \frac{Sk + n^{1/2}}{Sk + \Gamma_m}, \tag{3.16}$$

where S is an arbitrary coefficient, will tend to unity in both the limits $k \ll 1$ and $k \gg 1$.

4. Numerical solution

Equations (3.6) were integrated in the range $0.001 \leqslant \bar{z} \leqslant 5.0$ using the fourth-order Runge–Kutta method with step size $\Delta\bar{z} = 0.001$.

Initial conditions for the numerical solution were generated by first choosing a small value of k (here 0.1) and hence the corresponding value of $\bar{A}$. The choice of Γ_0 then sets the initial value of $\bar{w}$ using (3.14), and hence also $\bar{V}$. Here, the pure-plume initial condition of $\Gamma_0 = 1$ was considered, as well the forced-plume initial condition of $\Gamma_0 = 0.5$. It can be seen from (3.14) that this latter condition corresponds to a plume source with an initial momentum flux approximately 30 % greater than the equivalent for a pure plume.

Thus far, x_0 has not been specified relative to the other length scales in the problem. Following the approach of previous studies, x_0 is now taken to be the diameter of the circle on which the sources are placed, so that the value of $\bar{R}$ becomes 0.5.

For $k = 0.1$, the initial radius b_0 of each plume source at the first model level $\bar{z}_1 = 0.001$ is given approximately by the limiting value at small values of k, i.e. $b_0 = 0.1R/n$, and hence $2b_0/x_0 = 0.1/n$ (since $R = x_0/2$). If the pure-plume similarity solution for radius $b = 6\alpha z/5$ (Morton, Taylor & Turner 1956) is used to estimate the displacement in the negative z direction of the virtual origin $\bar{z}_{vn}$ for the source plumes, then

$$\bar{z}_{vn} + \bar{z}_1 \approx \frac{5}{6}\left(\frac{0.05}{n}\right). \tag{4.1}$$

Hence $\bar{z}_{vn} \approx 0.042n^{-1} - 0.001$. Thus $\bar{z}_{vn} \approx 0.02$ for the important case $n = 2$. It should be emphasised that this is the virtual origin correction for the individual plumes in the near field, and hence for the numerical solution. It is not the appropriate virtual origin correction for modelling analytically the far-field flow in terms of a single plume.

The results for $n = 2$ are plotted as the dashed lines in figure 3. The near- and far-field similarity solutions are also shown (dotted, see § 3.2), and are approached by the model solution at small and large $\bar{z}$, respectively. The numerical solutions include the correction $\bar{z}_{vn}$ for the near-field virtual origin, which greatly improves the similarity scaling at small $\bar{z}$.

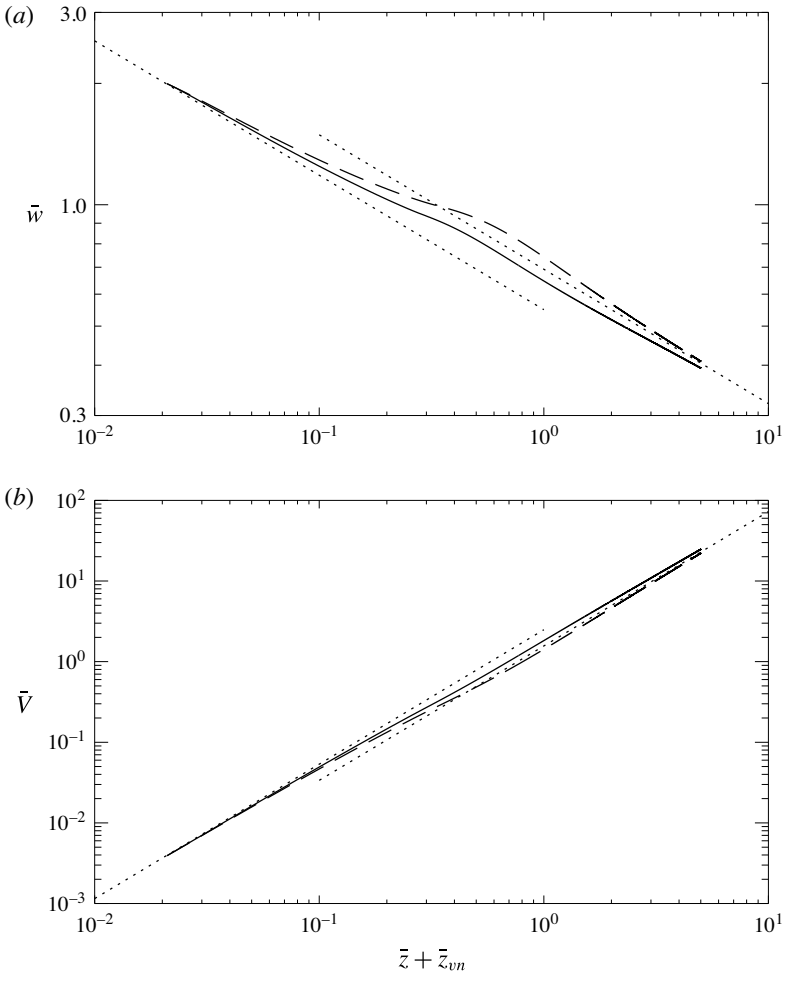

FIGURE 3. Solutions for $\bar{w}$ (*a*) and $\bar{V}$ (*b*) from the original model (dashed) and the revised model (solid), for the case $n=2$. The dotted lines show the near- and far-field similarity solutions, at lower and higher ranges of $\bar{z}+\bar{z}_{vn}$, respectively.

From (3.11) it can be seen that, in the far field, the horizontal plume length scale $\bar{A}^{1/2} = (\bar{V}/\bar{w})^{1/2}$ increases linearly with $\bar{z}$, i.e. the far-field plume is straight sided. The dimensionless far-field virtual origin $\bar{z}_{vf}$ may thus be calculated by fitting a straight line to the graph of $\bar{z}$ against $(\bar{V}/\bar{w})^{1/2}$ for data in the far field (taken here as $3 < \bar{z} \leqslant 5$), and extrapolating back to the intersect with the $\bar{z}$-axis. Figure 4 shows examples of this procedure. The results for the first few values of n, as well as the height of first contact, are given in table 1. The height of first contact is that at which $k=1$, when the velocity-potential contour defining the sector plume boundary reaches the origin, see figure 2. The model prediction of the distance to the position of first contact for two plumes is $\bar{z} = 0.31$ which is comparable ($\sim$90 %) to that of Cenedese & Linden (2014).

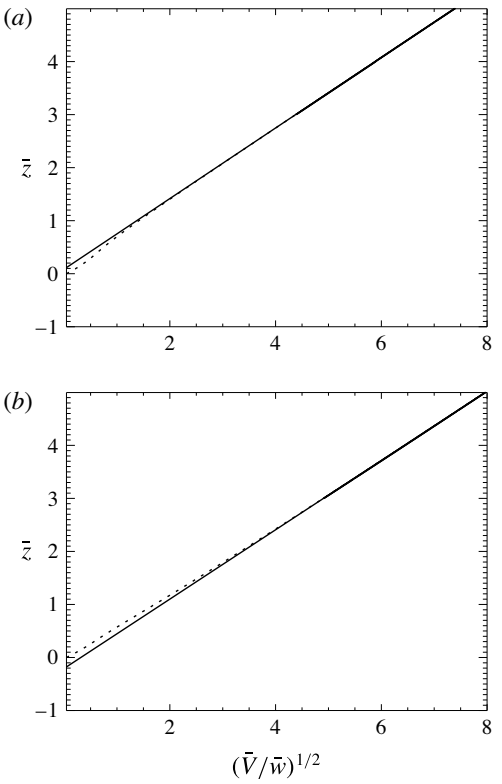

FIGURE 4. Determination of the far-field virtual origin $\bar{z}_{vf}$ for the case $n = 2$, with the original (*a*) and revised (*b*) models. The dotted lines show the data from the model integration, and the solid lines show straight line fits to the data between $3 < \bar{z} \leqslant 5$. Extrapolation of the fit backward to the $\bar{z}$ axis provides the value of $\bar{z}_{vf}$. Note that the axis intersect in (*a*) is 'in front of' the plume origin, so $\bar{z}_{vf}$ is negative for this case in table 1, and *vice versa* for (*b*). Equivalent plots for other values of n are similar to those shown.

n	2		3		4		5	
Model	Original	Revised	Original	Revised	Original	Revised	Original	Revised
$\bar{z}_{vf}$	−0.11	0.19	−0.08	0.25	−0.06	0.22	−0.05	0.20
$\bar{z}$ at $k = 1$	0.31	0.28	0.28	0.23	0.27	0.21	0.26	0.20

TABLE 1. Predictions for the offset behind the actual origin of the far-field virtual origin, and for the point of first contact ($k = 1$), in the original and revised model formulations. Results are presented for different numbers of plumes n. The data include small corrections for the near-field virtual origin $\bar{z}_{vn}$, obtained from (4.1).

5. Behaviour in the merging region

5.1. *Evolution of* Γ_m

In the limit of $k \ll 1$ the plumes may be assumed to influence each other relatively little, and in the limit of $k \gg 1$ the merged plume should be similar to the far field

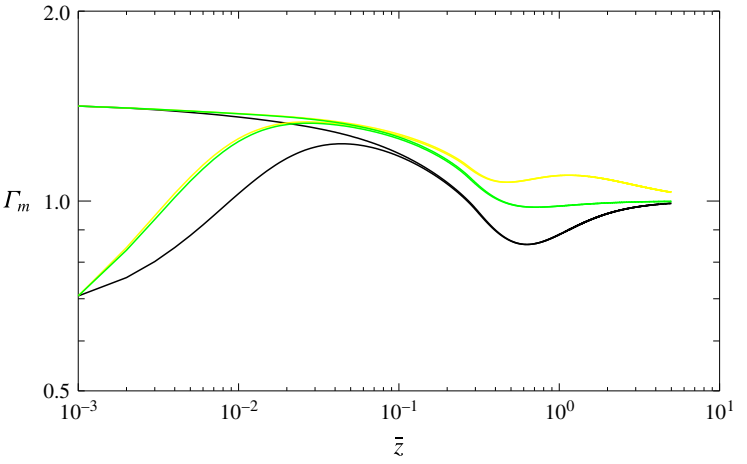

FIGURE 5. Behaviour of the flux-balance parameter Γ_m in the case $n = 2$, for different values of the single-plume source parameter Γ_0 and different entrainment models. The initial integration condition is either $\Gamma_0 = 1$ or $\Gamma_0 = 0.5$, corresponding to pure or slightly forced individual plumes, respectively. The initial values of Γ_m are then $2^{1/2}\Gamma_0$ in both cases. The colours correspond to 'simple' entrainment (black), and enhanced merging entrainment with $S = 1$ (green) or $S = 0.1$ (yellow).

of a plume from a single source. Model behaviour in these limits is thus quite tightly constrained to emulate the well-described single-plume model, and it has been shown in § 3 that these limits are represented satisfactorily (see also figure 3).

In the merging region, plume behaviour is less well understood, and consequently there is less available guidance to constrain aspects of the model such as entrainment. The simplest entrainment assumption (3.2) assumes that the entrainment velocity at the outer plume boundary on the line of symmetry $\theta = 0$, denoted q_e, should be proportional to the top-hat vertical velocity w. The implications of this assumption in the merging region may be assessed by examining the evolution of the flux-balance parameter Γ_m. Recall from § 3 that it is expected that

$$\Gamma_m \longrightarrow \begin{cases} 1, & k \gg 1 \\ n^{1/2}\Gamma, & k \ll 1. \end{cases} \tag{5.1}$$

Figure 5 shows the evolution of Γ_m in the case $n = 2$. The black lines show the behaviour of the model with the entrainment assumption (3.2), and two different initial conditions of Γ_0 equal to 1 or 0.5. In the early part of the model evolution (approximately $\bar{z} \leqslant 0.1$), the plumes have not yet merged. The pure-plume run ($\Gamma_0 = 1$) maintains a value close to $\Gamma_m = 2^{1/2}$ while the forced-plume run ($\Gamma_0 = 0.5$) begins to tend towards this value. As the plumes increasingly influence each other, the value of Γ_m begins to reduce and finally tends ($\bar{z} \gg 1$) to the appropriate merged-plume value of 1.

However, the trajectory of Γ_m from one limit to the other shows a pronounced 'dip' to forced-plume (<1) values in the merging region (approximately $0.1 \leqslant \bar{z} \leqslant 1$). The implication of this dip is that the plume entrainment is relatively low in the merging region, allowing the plume to accelerate rather than tend smoothly to the final limit. This may also be observed in figure 3(*a*), where the simple entrainment model

(dashed line) climbs above the far-field similarity solution (dotted line) before tending back down to it for larger values of $\bar{z}$. As has been emphasised above, there is little detailed observational data on the merging region to constrain the model, nonetheless this large departure from monotonicity is surprising, and indicates that the simple entrainment assumption may need modification.

5.2. *Modified entrainment assumption*

The simplest entrainment assumption, namely a constant value of α, has been observed to work well for pure plumes in both axisymmetric and two-dimensional configurations (Turner 1969). It has, however, required modification to reconcile models with data in many non-pure or transitional regimes. This is usually achieved through the dependence of α on a dimensionless parameter. These regimes include forced plumes (Wang & Law 2002), non-Boussinesq plumes (Rooney & Linden 1996) and turbulent fountains with a viscosity differing from that of the environment (Campbell & Turner 1985). The physical or dynamical reasons for these observed dependencies are still a subject of debate and research (e.g. Ezzamel, Salizzoni & Hunt 2015; van Reeuwijk & Craske 2015). For the case of plumes merging in a line, Rooney (2015) obtained good first-order agreement with experimental data without varying α. In that work, however, the possibility of developing the merging-plume model further by relating the value of α to a transitional parameter (such as the plume boundary curvature) was raised, should better experimental data become available. In the present case, some detailed data have been presented recently by Cenedese & Linden (2014).

If the plume is in some sense self-regulating, as the evolution of Γ for a single plume with arbitrary source conditions would suggest, then it is natural to modify the merging entrainment based on the value of Γ_m. This may be achieved using a function such as f_m (3.16) to scale the entrainment constant. This function tends to unity in the limit of large k, and also in the limit of small k for pure initial plumes. Thus the near- and far-field similarity behaviour is preserved. It also has Γ_m in the denominator, thus will regulate the merging by increasing entrainment when Γ_m is lower and *vice versa*. The modified entrainment assumption then becomes

$$q_e = \alpha f_m w. \tag{5.2}$$

At this stage, the form of the function and the value of S are otherwise arbitrary, but may be assessed by comparison with previous model behaviour and (in § 6, following) with the available observations.

To compare the modified model with the simple entrainment model, figure 5 also shows the behaviour of Γ_m in the modified case for values of $S = 1$ (green lines) and $S = 0.1$ (yellow lines). For $S = 1$, the far-field evolution only slightly dips below the $\Gamma_m = 1$ line, while for $S = 0.1$ the far-field values remain above $\Gamma_m = 1$. In this latter case the behaviour for pure initial plumes, while not entirely monotonic, no longer oscillates around the far-field pure-plume solution. This behaviour is probably more to be expected than that of the simple entrainment model. The results from the rest of this section will be based on the revised model with $S = 0.1$, $\Gamma_0 = 1$.

Figure 6 compares the effective entrainment in the two models according to (3.10), with the simple model dashed and the revised model solid black. it also shows the effective entrainment from the piecewise merging model of Cenedese & Linden (2014) in red. The piecewise model does not reduce plume entrainment below the merging region however, outside this region, the revised entrainment model produces an effective entrainment closer to that of Cenedese & Linden (2014).

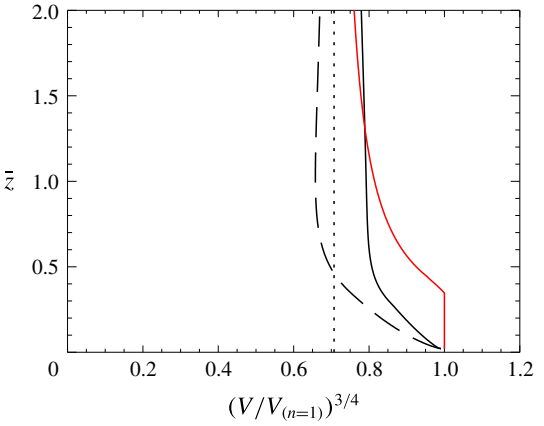

FIGURE 6. Effective entrainment of two merging plumes compared to that of two isolated plumes, see (3.10) and the accompanying text. The flux ratio from the simple model is dashed, and that from the revised model is solid black. The piecewise model of Cenedese & Linden (2014, equation (2.12)) is shown in red for comparison. The vertical dotted line indicates the value of $2^{-1/2}$, to which all the two-plume models tend in the far field.

The numerical solution of the model with the modified entrainment assumption is shown by the black solid lines in figure 3. It can be seen that $\bar{w}$ and $\bar{V}$ now evolve from the single-plume to the merged-plume values without overshooting the merged-plume similarity solution. In the far field, the modified model has a greater volume flux and lower vertical velocity than the original. The merging of three plumes using this model is illustrated in figure 7.

The far-field virtual origin $\bar{z}_{vf}$ and the height of first contact obtained from the modified model are given alongside those from the original model formulation in table 1. The change of $\bar{z}_{vf}$ to positive values, i.e. positions behind the plume origin, is a result of the increased volume flux due to the greater merging entrainment. For two plumes, the model of Kaye & Linden (2004) predicted a value of $z_{vf}/x_0 = 1.4$, and their experiments showed agreement with this. The revised $n = 2$ prediction of $\bar{z}_{vf} = 0.19$, with a value of $\alpha = 0.12$ (Cenedese & Linden 2014, discussed further in the next section), would imply $z_{vf}/x_0 \approx 1.6$, which is then comparable with the experimental value of Kaye & Linden (2004).

The revised model for two plumes reduces the height of first contact ($\bar{z} = 0.28$) to approximately 80 % of that of the model of Cenedese & Linden (2014). Nonetheless, the distances remain of a similar magnitude. It may also be noted that this distance shows indications of being lower in some other modelling or experimental studies e.g. Lai & Lee (2012, figure 9*a*) and Kaye & Linden (2004, figure 13).

6. Merging-plume volume flux

In this section, the volume-flux predictions of the models for the case $n = 2$ are compared with that inferred from observations of a 'filling-box' experiment by Cenedese & Linden (2014). In that experiment, two salt water sources discharged into a tank of fresh water, creating a layer of salt water at the bottom of the tank, see figure 8. Each source produced a buoyancy flux B, and the initially separate plumes eventually merged into one.

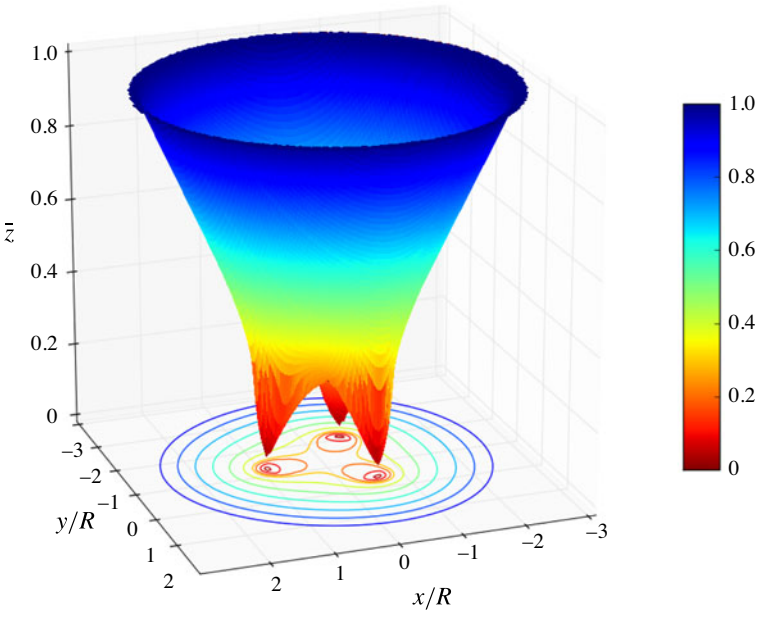

FIGURE 7. An illustration of the merging of three plumes, obtained with the modified model. The numerical solution gives the mapping between $\bar{z}$ and k, and thus the locus of the plume boundary at any height, from (2.6). To help with visualisation, the plume system is shaded according to the height $\bar{z}$ in the range between 0 and 1, and shaded contours are also projected onto the bottom plane.

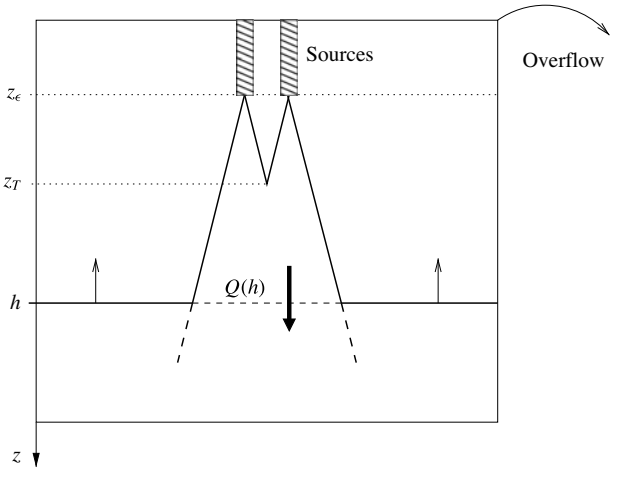

FIGURE 8. The experiment of Cenedese & Linden (2014), in which salt water plumes from two sources at the same height produce a depth-dependent volume flux Q. This fills a tank of fresh water by displacement. The fresh–salty interface is at depth $h(t)$. The plumes are observed to touch at depth z_T and z_ϵ denotes a position very close to the source.

The analysis of Cenedese & Linden (2014) must first be outlined. This proceeds by relating the interface position h to the total salt-plume volume flux $Q(z=h)$ and the horizontal area of the tank interior A_i (where z is the vertical coordinate measured downward from the source level),

$$Q(h) = -A_i \frac{\partial h}{\partial t}, \tag{6.1}$$

and the area of the interface occupied by the plumes is assumed small enough to be neglected. If the plumes are observed to touch at some (constant) level z_T, then the time taken for the interface to reach z_T from some arbitrary point (z, t) is obtained from

$$\frac{t_T - t}{A_i} = \int_{z_T}^{z} \frac{\mathrm{d}z^*}{Q}, \tag{6.2}$$

where t_T is the time at which z_T is reached. Using the dimensionless time coordinate

$$\tau = \frac{t_T - t}{A_i x_0^{-2/3} B^{-1/3}}, \tag{6.3}$$

then (6.2) becomes

$$\tau = \int_{\bar{z}_T}^{\bar{z}} \frac{\mathrm{d}\bar{z}^*}{\alpha^{2/3}\bar{Q}}, \tag{6.4}$$

where Q and z have been non-dimensionalised as in (3.5). Cenedese & Linden (2014) use the value of $\bar{z}_T = 0.35$ as predicted by their piecewise merging model.

For n plumes, $\bar{Q} = n\bar{V}$ so that, from (3.11*b*) and the following discussion,

$$\bar{Q} \to \begin{cases} n\dfrac{6}{5}\left(\dfrac{9}{10}\right)^{1/3}\left(\dfrac{n}{\pi}\right)^{-2/3}(\bar{z}+\bar{z}_{vf})^{5/3}, & k \gg 1 \\ n\dfrac{6}{5}\left(\dfrac{9}{10}\right)^{1/3}\pi^{2/3}\bar{z}^{5/3}, & k \ll 1, \end{cases} \tag{6.5}$$

where $\bar{z}_{vf}$ is the appropriate virtual origin for the far field, and the near-field virtual origin is neglected. Thus for $n = 2$

$$\tau \approx \begin{cases} \dfrac{3}{2^{4/3}}\left(\dfrac{6}{5}\left(\dfrac{9}{10}\right)^{1/3}\pi^{2/3}\alpha^{2/3}\right)^{-1}((\bar{z}_T+\bar{z}_{vf})^{-2/3} - (\bar{z}+\bar{z}_{vf})^{-2/3}), & z > z_T \\ \dfrac{3}{4}\left(\dfrac{6}{5}\left(\dfrac{9}{10}\right)^{1/3}\pi^{2/3}\alpha^{2/3}\right)^{-1}(\bar{z}_T^{-2/3} - \bar{z}^{-2/3}), & z < z_T. \end{cases} \tag{6.6}$$

Equation (6.6) is essentially the τ–$\bar{z}$ relationship derived by Cenedese & Linden (2014), but neglecting the separate linear fit in the merging region. For the purposes of the present comparison, it provides a close fit to the non-dimensionalised data from that study, upon using the value $\bar{z}_{vf} = 0.12$.

The time taken for the interface to travel from z_T to almost the plume origin is given by

$$\Delta\tau = \frac{t_\epsilon - t_T}{A_i x_0^{-2/3} B^{-1/3}} = \int_{\bar{z}_\epsilon}^{\bar{z}_T} \frac{\mathrm{d}\bar{z}^*}{\alpha^{2/3}\bar{Q}}, \tag{6.7}$$

where (z_ϵ, t_ϵ) is the event arbitrarily close to the plume source. To compare the numerical solution with the results of Cenedese & Linden (2014), $\bar{z}_\epsilon$ can be taken as $\bar{z}_1 = 0.001$ and also $\bar{z}_T = 0.35$, and hence τ is calculated from the model solution as

$$\tau = \int_{\bar{z}_1}^{\bar{z}} \frac{\mathrm{d}\bar{z}^*}{\alpha^{2/3}\bar{Q}} - \Delta\tau. \tag{6.8}$$

One possible effect neglected by this analysis is additional entrainment into the lower layer which may occur when the plume passes through the interface (Cetegen, Zukoski & Kubota 1984). If this is significant, then the interface movement may reflect a greater volume flux than that in the underlying plume flow.

Figure 9 shows results plotted in $(\tau, \bar{z})$-space. It should be noted that this way of presenting the results is quite sensitive to the values of α and $\bar{z}_{vf}$. Cenedese & Linden (2014) do not state their measured value of α but their plot of dimensionless data is consistent with a value of $\alpha \approx 0.12$. The far-field similarity solution (6.6, $z > z_T$), with $\bar{z}_{vf} = 0.12$, is the red line in the region $\tau > 0$. The near-field similarity solution (6.6, $z < z_T$) is the magenta line in the region $\tau < 0$. These lines, plotted using $\alpha = 0.12$, are a good fit to the scaled experimental data in the plotting range shown. The model with the simple entrainment assumption (3.2) and assuming $\Gamma_0 = 1$, $\alpha = 0.12$, is shown as the black dashed line, which does not appear to follow the data at larger values of $\bar{z}$. For the model with the modified entrainment assumption (5.2), a range of solutions is shown by the grey shaded region, covering the likely range of uncertainty in the model and experiments, i.e. $0.10 \leqslant \alpha \leqslant 0.14$, $0.5 \leqslant \Gamma_0 \leqslant 1$, $0.1 \leqslant S \leqslant 1$. This region is bounded by the green and yellow lines, which correspond to parameter values of $(\alpha = 0.10,\ \Gamma_0 = 1,\ S = 1)$ and $(\alpha = 0.14,\ \Gamma_0 = 0.5,\ S = 0.1)$, respectively. For the second of these, the analysis of Hunt & Kaye (2001) indicates that the near-field virtual origin should be increased slightly to $\bar{z}_{vn} \approx 0.03$. The small radius of the plume source relative to the domain size means that virtual origin corrections are also small, so that in general the offset by $\bar{z}_{vn}$ does not greatly affect the positions of the curves in this plot.

It appears from figure 9 that the experimental data can be matched by the model from the parameter values considered, although they are at one end of the parameter range. This may be due in part to the possible effect of extra interfacial entrainment, mentioned above.

7. Conclusion

The preceding sections have developed a model to represent merging of a circular array of plumes. This model yields the correct similarity behaviour in the near and far fields, and includes continuously varying plume entrainment and boundary shape from the plume source to the far-field flow.

The formulation of the model has included plume distortion as the main process of plume interaction in the merging region. It has been shown that this is sufficient to represent the drawing together of plumes within a distance from the source comparable to previous observations. Plume distortion removes the 'cusp' in merging-plume cross-sections which is a feature of overlapping-axisymmetric plume models. It also ensures that the irrotational entrainment field is self-consistent and normal to the plume boundary at all points.

Consideration of the flux-balance parameter Γ_m has been used to highlight the tendency of the simplest entrainment assumption to insufficiently decelerate the

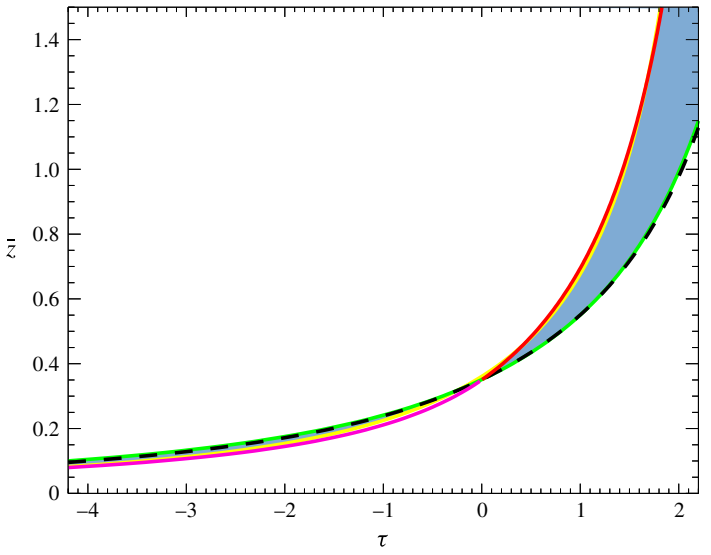

FIGURE 9. Comparison of model output with the experimental data of Cenedese & Linden (2014). The red and magenta lines are integrations of the far- and near-field similarity solutions, respectively ((6.6), taking $\bar{z}_{vf} = 0.12$ in the former), and also indicate the trajectory of the scaled experimental data. The dashed black line shows the original model with the default parameter settings. The grey shading shows the range of revised model results over the parameter ranges considered, with the green and yellow lines indicating model results at the range limits (explained in the text).

merging plumes. It has also allowed the formulation of a revised merging entrainment assumption which regulates this behaviour. The revised model has been shown to yield results which compare satisfactorily with inferred estimates of volume flux in the merging zone of two plumes, within the ranges of experimental and model uncertainty.

Finally, a remark may be made concerning the application to a plume in a corner of arbitrary angle. It is expected that corners of size $2\pi/n$ where n is non-integer may be described approximately by interpolating the integer results in table 1, for example. It is interesting to note that the velocity potential from (2.2) may be plotted for non-integer n, and varies smoothly in the sector containing unity. However, a discontinuity appears along the negative real axis, since the potential field is now periodic on an interval no longer equal to 2π. This indicates that the plume-analogous configuration for non-integer cases is yet to be fully understood.

Appendix A. Entrainment-flux integrals

The flux E across a contour C is (2.17),

$$E = \int_C q \, \mathrm{d}\ell = \frac{mI}{2\pi}, \tag{A 1}$$

where

$$I = \int_C \frac{2\pi R\, q}{m} \, \mathrm{d}\ell' = \frac{n}{k} \int_C \rho^{n-1} \, \mathrm{d}\ell'. \tag{A 2}$$

For contour integration, it is useful to express $\mathrm{d}\rho/\mathrm{d}\theta$ in terms of either ρ or θ only. From (2.5) and its simplifications (2.6) and (2.7), (2.8) becomes

$$\begin{aligned}\frac{\mathrm{d}\rho}{\mathrm{d}\theta} &= \frac{\rho(4\rho^{2n}-(\rho^{2n}+1-k^2)^2)^{1/2}}{1-\rho^{2n}-k^2}\\ &= \mp\frac{\sin n\theta(\cos n\theta \pm (k^2-\sin^2 n\theta)^{1/2})^{1/n}}{(k^2-\sin^2 n\theta)^{1/2}}.\end{aligned} \tag{A 3}$$

Now from (2.16),

$$\begin{aligned}\mathrm{d}\ell'^2 &= \left(1+\rho^2\left(\frac{\mathrm{d}\theta}{\mathrm{d}\rho}\right)^2\right)\mathrm{d}\rho^2\\ &= \left(\left(\frac{\mathrm{d}\rho}{\mathrm{d}\theta}\right)^2+\rho^2\right)\mathrm{d}\theta^2,\end{aligned} \tag{A 4}$$

and so using (2.6) and (A 3),

$$\begin{aligned}\mathrm{d}\ell' &= \frac{2k\rho^n}{(4\rho^{2n}-(\rho^{2n}+1-k^2)^2)^{1/2}}\,\mathrm{d}\rho\\ &= \frac{k(\cos n\theta \pm (k^2-\sin^2 n\theta)^{1/2})^{1/n}}{(k^2-\sin^2 n\theta)^{1/2}}\,\mathrm{d}\theta.\end{aligned} \tag{A 5}$$

For open contours ($k>1$), again using (2.6), the entrainment flux is then an angular integral over the whole sector,

$$I = n\int_{-\pi/n}^{\pi/n}\frac{\cos n\theta+(k^2-\sin^2 n\theta)^{1/2}}{(k^2-\sin^2 n\theta)^{1/2}}\,\mathrm{d}\theta = 2\pi. \tag{A 6}$$

For closed contours ($k\leqslant 1$), one half of the flux may be obtained as a radial integral,

$$\frac{I}{2} = 2n\int_{\rho_{min}}^{\rho_{max}}\frac{\rho^{2n-1}}{(4\rho^{2n}-(\rho^{2n}+1-k^2)^2)^{1/2}}\,\mathrm{d}\rho. \tag{A 7}$$

Making the substitution $\chi=\rho^{2n}+1-k^2$ produces

$$\begin{aligned}I &= 2\int_{2-2k}^{2+2k}\frac{\mathrm{d}\chi}{(-\chi^2+4\chi+4k^2-4)^{1/2}}\\ &= 2\left[-\sin^{-1}\left(\frac{4-2\chi}{4k}\right)\right]_{2-2k}^{2+2k}\\ &= 2\pi.\end{aligned} \tag{A 8}$$

Hence $E=m$ in all cases, which is perhaps not unexpected.

REFERENCES

ALESSANDRINI, S., FERRERO, E. & ANFOSSI, D. 2013 A new Lagrangian method for modelling the buoyant plume rise. *Atmos. Environ.* **77**, 239–249.

BABRAUSKAS, V. 1980 Flame lengths under ceilings. *Fire Mater.* **4** (3), 119–126.

BATCHELOR, G. K. 1967 *An Introduction to Fluid Dynamics*. Cambridge University Press.

CAMPBELL, I. H. & TURNER, J. S. 1985 Turbulent mixing between fluids with different viscosities. *Nature* **313**, 39–42.

CENEDESE, C. & LINDEN, P. F. 2014 Entrainment in two coalescing axisymmetric turbulent plumes. *J. Fluid Mech.* **752**, R2.

CETEGEN, B. M., ZUKOSKI, E. E. & KUBOTA, T. 1984 Entrainment in the near and far field of fire plumes. *Combust. Sci. Technol.* **39**, 305–331.

DAVIDSON, M. J., PAPPS, D. A. & WOOD, I. R. 1994 The behaviour of merging buoyant jets. In *Recent Research Advances in the Fluid Mechanics of Turbulent Jets and Plumes* (ed. P. A. Davies & M. J. V. Neves), NATO ASI Series, vol. 255, pp. 465–478. Springer.

EZZAMEL, A., SALIZZONI, P. & HUNT, G. R. 2015 Dynamical variability of axisymmetric buoyant plumes. *J. Fluid Mech.* **765**, 576–611.

HUNT, G. R. & KAYE, N. B. 2005 Lazy plumes. *J. Fluid Mech.* **533**, 329–338.

HUNT, G. R. & KAYE, N. G. 2001 Virtual origin correction for lazy turbulent plumes. *J. Fluid Mech.* **435**, 377–396.

KAYE, N. B. & LINDEN, P. F. 2004 Coalescing axisymmetric turbulent plumes. *J. Fluid Mech.* **502**, 41–63.

KIMURA, S., HOLLAND, P. R., JENKINS, A. & PIGGOTT, M. 2014 The effect of meltwater plumes on the melting of a vertical glacier face. *J. Phys. Oceanogr.* **44**, 3099–3117.

LAI, A. C. H. & LEE, J. H. W. 2012 Dynamic interaction of multiple buoyant jets. *J. Fluid Mech.* **708**, 539–575.

LINDEN, P. F., LANE-SERFF, G. F. & SMEED, D. A. 1990 Emptying filling boxes: the fluid mechanics of natural ventilation. *J. Fluid Mech.* **212**, 309–335.

MOKHTARZADEH-DEHGHAN, M. R., KÖNIG, C. S. & ROBINS, A. G. 2006 Numerical study of single and two interacting turbulent plumes in atmospheric cross flow. *Atmos. Environ.* **40** (21), 3909–3923.

MORTON, B. R., TAYLOR, G. I. & TURNER, J. S. 1956 Turbulent gravitational convection from maintained and instantaneous sources. *Proc. R. Soc. Lond.* A **234**, 1–23.

VAN REEUWIJK, M. & CRASKE, J. 2015 Energy-consistent entrainment relations for jets and plumes. *J. Fluid Mech.* **782**, 333–355.

ROONEY, G. G. 2015 Merging of a row of plumes or jets with an application to plume rise in a channel. *J. Fluid Mech.* **771**, R1.

ROONEY, G. G. & LINDEN, P. F. 1996 Similarity considerations for non-Boussinesq plumes in an unstratified environment. *J. Fluid Mech.* **318**, 237–250.

TAYLOR, G. I. 1958 Flow induced by jets. *J. Aero. Sci.* **25**, 464–465.

TURNER, J. S. 1969 Buoyant plumes and thermals. *Annu. Rev. Fluid Mech.* **1**, 29–44.

TURNER, J. S. 1973 *Buoyancy Effects in Fluids*. Cambridge University Press.

WANG, H. & LAW, A. W.-K. 2002 Second-order integral model for a round turbulent buoyant jet. *J. Fluid Mech.* **459**, 397–428.

YANNOPOULOS, P. 2010 Advanced integral model for groups of interacting round turbulent buoyant jets. *Environ. Fluid Mech.* **10** (4), 415–450.